Conformationally Constrained Peptides with High Affinity to the Vascular Endothelial Growth Factor

Guryanov, Ivan

2021-08-12

Guryanov , I , Korzhikov-Vlakh , V , Bhattacharya , M , Biondi , B , Masiero , G , Formaggio , F , Tennikova , T & Urtti , A 2021 , ' Conformationally Constrained Peptides with High Affinity to the Vascular Endothelial Growth Factor ' , Journal of Medicinal Chemistry , vol. 64 , no. 15 , pp. 10900-10907 . https://doi.org/10.1021/acs.jmedchem.1c00219

http://hdl.handle.net/10138/346912
https://doi.org/10.1021/acs.jmedchem.1c00219

acceptedVersion

Conformationally Constrained Peptides with High Affinity to Vascular Endothelial Growth Factor

Ivan Guryanov,[§,*] Viktor Korzhikov-Vlakh,[§] Madhushree Bhattacharya,[‖] Barbara Biondi,[#] Giulia Masiero,[#] Fernando Formaggio,[#] Tatiana Tennikova,[§] and Arto Urtti[‖]

[§]Institute of Chemistry, St. Petersburg State University, Universitetsky pr. 26, 198504 St. Petersburg, Peterhof, Russia

[#]ICB, Padova Unit, CNR, Department of Chemistry, University of Padova, via Marzolo 1, 35131 Padova, Italy

[‖]Centre for Drug Research, Division of Pharmaceutical Biosciences, University of Helsinki, Viikinkaari 5 E, FIN-00014 Helsinki, Finland

The design of efficient vascular endothelial growth factor (VEGF) inhibitors is a high priority research area aimed at the treatment of pathological angiogenesis. Among other compounds, **v114*** has been identified as very potent VEGF-binding peptide. In order to improve its affinity to VEGF, we built a conformational constrain in its structure. To this aim C^{α}-tetrasubstituted amino acid Aib was introduced into N-terminal tail, peptide loop and C-terminal helix. NMR studies confirmed the stabilization of helical conformation in the proximity to Aib residue. We found that the induction of N-terminal helical structure or stabilization of the C-terminal helix can noticeably increase the peptide affinity to VEGF. These peptides efficiently inhibited VEGF-stimulated cell proliferation as well. The insertion of non-proteinogenic Aib residue significantly enhanced the stability of the peptides in vitreal environment of the eye. Thus, these Aib-containing peptides are promising candidates for the design of VEGF inhibitors with improved properties.

KEYWORDS: VEGF, peptide, affinity, Aib, helix, inhibitor

INTRODUCTION

Vascular endothelial growth factor (VEGF) is one of the main regulators of the angiogenesis.[1] Unregulated expression of this protein causes proliferation and migration of the endothelial cells and uncontrolled growth of micro vessels in various tissues (pathological angiogenesis). This phenomenon contributes to the pathogenesis of a number of diseases, such as tumor growth, psoriasis, arthritis and age-related macular degeneration (AMD).[2] The main reason of wet form of AMD is the VEGF-dependent increase in vascular permeability and retinal pigment epithelial detachment, that account for over 90% of the cases with severe visual loss with many complications, such as subretinal and vitreous hemorrhage, fibrosis, and scarring.[3] The number of patients with AMD is expected to reach 288 millions world-wide in 2040.[4] Though a noticeable advances in AMD treatment have been achieved over the last years, the development of novel and improved therapeutic strategies remains highly requested.

There are various possibilities to control the activity of VEGF-dependent signaling pathways: inhibition of the endogenous secretion of VEGF; neutralizing VEGF with oligonucleotides, antibodies, and VEGF binding extracellular receptor domains; low molecular weight inhibitors of the VEGF receptor interaction.[5,6] Among compounds developed so far antibodies (mAbs) and soluble receptors (decoy receptors) are the most widespread in AMD therapy. Bevacizumab (Avastin®), ranibizumab (Lucentis®) and pegaptanib (Macugen®) injections have been used extensively in ophthalmology for age-related macular degeneration, diabetic retinopathy, retinal vein occlusions, retinopathy of prematurity and other chorioretinal vascular disorders.[7] The full-length soluble receptor is currently used in medicine with the name aflibercept (Eylea®). Many attempts were made to design VEGF inhibitors based only on the binding domains of the VEGFR, such as VEGF-trap (Regeneron Pharmaceuticals, Inc), a chimeric fusion molecule, consisting of the second Ig domain of VEGFR-1 and the third domain VEGFR-2, fused to Fc portion of IgG1.[8]

Despite all the achievements in the treatment of AMD, the design of novel VEGF inhibitors remains a high priority research area, since many drawbacks are associated with the current pharmaceuticals. The anti-VEGF injections are given as a long-term treatment and constitute a significant burden for both patients and medical personnel. The fast elimination from the vitreous, suboptimal dosing frequency and the risk of complications, such as endophthalmitis, uveitis, vitreous haemorrhage, limit the use and patient compliance of the existing antiangiogenic therapy.[9] Effective long acting and/or minimally invasive drug delivery would noticeably improve ophthalmologic therapy. Furthermore, as significant fraction of the patient population responds poorly, new pharmaceutical options are needed.

From this point of view the design of small peptide VEGF inhibitors can be a promising approach for the development of novel pharmaceuticals with enhanced binding activity and stability for the treatment of VEGF-dependent diseases, including AMD.[10,11] Several short peptides, which could interact with VEGFR-binding surface of VEGF with high affinity and selectivity, have been described.[12,13] In particular, two promising cyclic helical anti-VEGF peptides **v107** (GGNEc[CDIARMWEWEC]FERL) and **v114** (VEPNc[CDIHVMWEWEC]FERL) with K_D values 0.53 and 0.11 μM, respectively, were identified by phage display technique. **V114***, in which the methionine residue was replaced by norleucine, was able to inhibit VEGF with a K_i as low as 60 nM (competitive fluorescence polarization assay). Alanine scans of **v107** and **v114** and "β-scan" of **v114*** revealed the sites in their peptide sequences involved in the interaction with VEGF molecule.[14] The extensive study of peptidomimetics based on **v114*** did not allow finding molecules with increased affinity and VEGF inhibition properties. However, it was concluded, that the reduction of its conformational freedom and the introduction of fluorination patterns to Phe16 may improve VEGF binding.[15]

In this study we introduced α-aminoisobutyric acid (Aib) residue into the amino acid sequence of **v114*** in order to reduce the flexibility of the peptide. Aib, as well as many other C^{α}-tetrasubstituted α-amino acids, is known to promote highly rigid and well developed folded structures even in the short peptides.[16-21] The creation of such conformational constrain can be particularly useful in the case of helical peptide **v114***. Moreover, the insertion of the non-proteinogenic Aib residue may increase the resistance to enzymatic degradation, that was successfully used for the creation of several peptide drugs, such as Semaglutide and Abaloparatide.[22,23]

RESULTS AND DISCUSSION

We introduced Aib residue in those sites of **v114*** amino acid sequence, which are not involved in the direct interaction with VEGF and are not crucial for its binding. Previously, it was shown that **v107** is strikingly amphipathic and in the complex with VEGF adopts mixed conformation with disordered N-tail (residues 1-4), type I β-turn (residues 6-9), extended region (residues 9-12) and C-terminal α-helix (residues 13-19), where hydrophobic Ile7, Ala8, Met10, Trp11, Trp13, Phe16 and Leu19 are situated on the interface with VEGF molecule (Figure 1).[24]

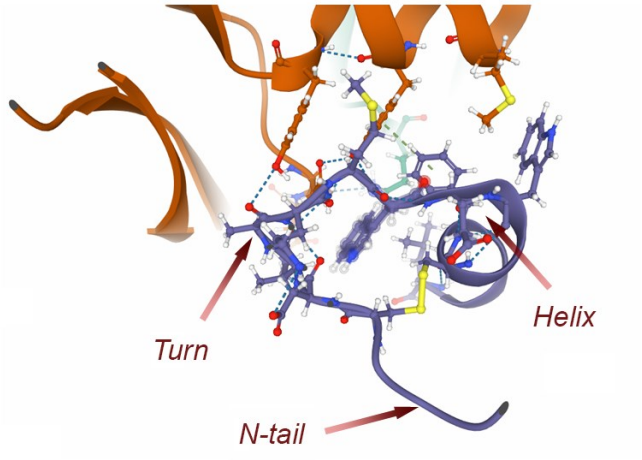

Figure 1. The structure of **v107** in VEGF-bound state and the sites in the peptide sequence suitable for Aib insertion (PDB: 1KAT).

The similarity of the amino acid sequences of **v107** and **v114*** allows supposing the resemblance of their conformation in the bound state. Therefore, for the modification we selected positions 8 and 12 in the peptide structure, where turn or helix rigidity, respectively, can increase the affinity to VEGF (Entries 3 and 4, Table 1).

Table 1. Amino acid sequences of v114* analogues

Entry	Abbreviation	Structure
1	**v114***	VEPNc[CDIHV^{n}LWEWEC]FERL-NH_2
2	**Aib2**	V**Aib**PNc[CDIHV^{n}LWEWEC]FERL-NH_2
3	**Aib8**	VEPNc[CDI**Aib**V^{n}LWEWEC]FERL-NH_2
4	**Aib12**	VEPNc[CDIHV^{n}LW**Aib**WEC]FERL-NH_2
5	**kv114***	K**Aib**KKc[CDIHV^{n}LWEWEC]FERL-NH_2
6	**sv114***	c[CDIHV^{n}LWEWEC]FERL-NH_2
7	**VN**	VNc[CDIHV^{n}LWEWEC]FERL-NH_2

We also studied the effects of N-terminal shortening (Entries 6 and 7, Table 1) and Aib insertion into the N-terminal tail (Entry 2, Table 1) on peptide rigidity and VEGF binding. Recently we showed that modification of the peptides with a short oligolysine sequence is an useful method for their non-covalent attachment and retention on the negatively charged surfaces of the nanoparticles covered by heparin layer.[25] Oligolysines can also enhance the binding of peptides to

the negatively charged cell surface and increase the elimination of the complex peptide/complementary ligand from the extracellular space by endocytosis. Here we extended this approach for the synthesis of anti-VEGF peptides. To this aim, along with the introduction of Aib, we substituted N-terminal amino acids of **v114*** by lysines, which could also slow down the elimination of the peptide from the vitreal environment due to the interaction with negatively charged hyaluronic acid of the vitreous (Table 1, Entry 5).

The preparation of the Aib-containing peptides is known to be rather complicated because of the steric hindrance of the α-aminoisobutyric acid. Therefore, the activation of its carboxylic group requires more efficient reagents than those commonly used. Thus, we introduced several modifications to the previously described procedure for the synthesis of Aib-containing analogs of **v114***.[14,15] In particular, Aib and the following amino acid were coupled by using HATU instead of HBTU, which allowed completion of the reaction with a good yield. Interestingly, in the case of **Aib2** the deletion peptide was separated as a main product, where Aib and Pro residues were lacking (peptide **VN**, Table 1). The inherent propensity of the -Aib-Pro- motif to form β-turn promoted the well-known intramolecular cyclization to diketopiperazine upon Fmoc-cleavage with piperidine (Figure S1).[26-28] In order to suppress this side reaction, Fmoc-removal was carried out in the presence of OxymaPure, which is able to protonate the forming amino group and, therefore, to decrease its nucleophilicity.[29] Thus, after cleavage of the peptide from the solid support and cyclization by air oxidation in a basic aqueous solution the target peptide was obtained with a good yield and purity (Table S1, Figure S2).

The 3D-structures of the peptides were extensively studied by circular dichroism (CD) spectroscopy.[30] In PBS solution the peptides adopted a mixed conformation with a remarkable content of helix and random coil, regardless of whether they contained Aib or not (Figure 2, A).

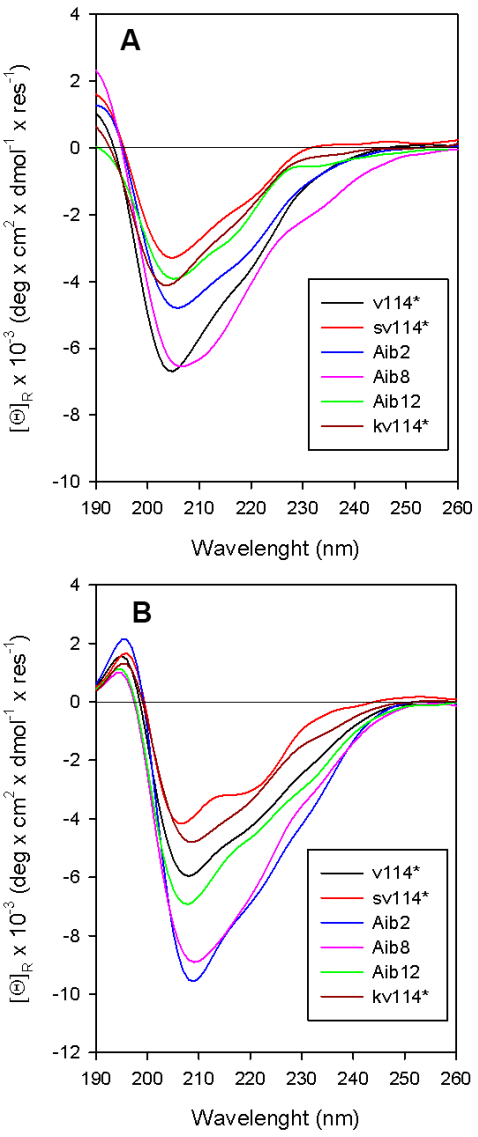

Figure 2. CD spectra of the peptides in PBS (A) and in methanol (B).

In methanol the helical structure was prevailing for all peptides (Figure 2, B). Indeed, in this organic solvent the negative π→π* transition moves to longer wavelengths, close to the canonical 208 nm of α-helix, and its negative maximum at 222 nm has a stronger intensity. **Kv114***, if compared to **Aib2**, had a lower tendency to assume the helical conformation, even though it had Aib residue in the same position. This is probably related to the repulsion of the three protonated N-terminal lysines.

More detailed information on the structure of the peptides was obtained from 2D-NMR spectra analysis. The fingerprint region of the NOESY spectrum of **v114*** in unbound state showed $C^{\alpha}H_i \rightarrow NH_{i+2}$, $C^{\alpha}H_i \rightarrow NH_{i+3}$ and $C^{\alpha}H_i \rightarrow NH_{i+4}$ cross peaks in the part of the peptide sequence that

comprised the amino acids from Cys5 to Phe16. The interactions Asp6/His8 and Cys5/Val9, as well as the signal arising from the proximity of Cys5 and Trp11, can be attributed to the formation of the loop at this peptide segment, followed by the C-terminal helix, the presence of which is evidenced by the interactions Trp13/Phe16 and Glu14/Glu12. No proton correlations were observed in the N-terminal part of the peptide (Figure 3, A).

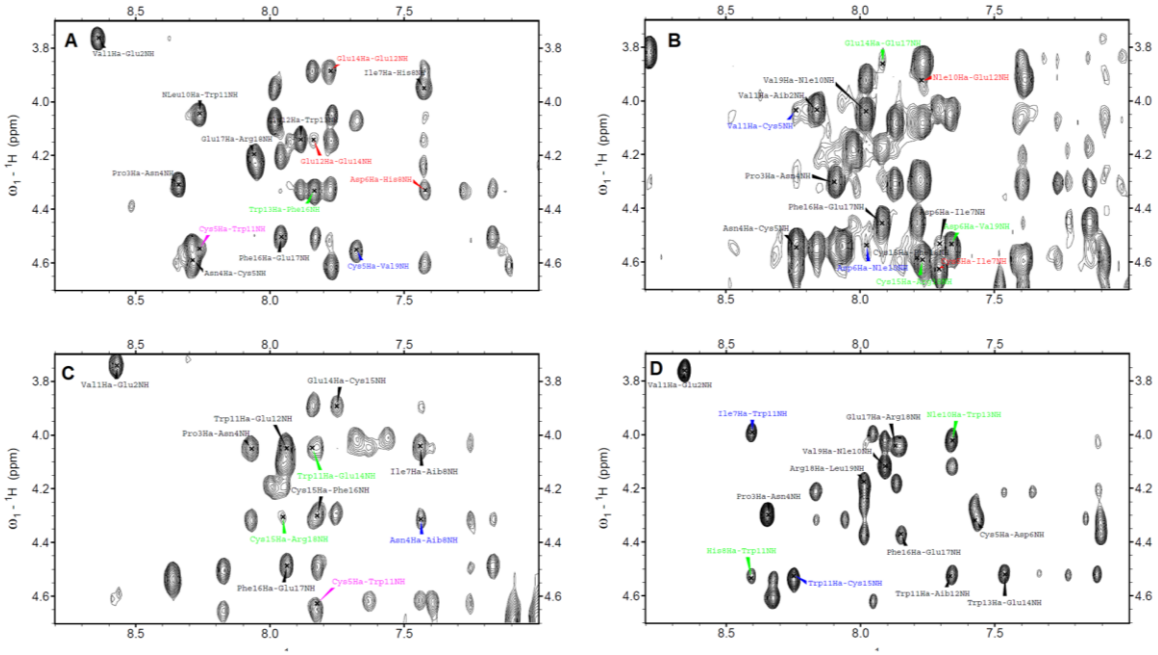

Figure 3. Fingerprint region of the NOESY spectrum of **v114*** (A), **Aib2** (B), **Aib8** (C), **Aib12** (D). Medium-range interactions are highlighted in red ($C^{\alpha}H_i \rightarrow NH_{i+2}$), green ($C^{\alpha}H_i \rightarrow NH_{i+3}$) and blue ($C^{\alpha}H_i \rightarrow NH_{i+4}$). The cross peak due to the interaction Cys5/Trp11 is evidenced in magenta.

Furthermore, the amide proton region exhibited the cross peaks characteristic of the presence of a helical conformation, which extended toward the C-terminal end of the peptide sequence (Figure S5). This is in agreement with the literature data[24] and confirms the similarity of spatial conformations for **v107** and **v114***.

The introduction of Aib into the amino acid sequence of the parent peptide **v114*** drastically changed its secondary structure. The fingerprint region of the NOESY spectrum of **Aib2** highlighted medium-range correlations typical of α-helix not only in the C-terminal part, but also in the N-terminal tail, starting from Val at position 1 (Figure 3, B). A similar pattern was also evident in the aliphatic/NH region, where a $C^{\beta}H_i \rightarrow NH_{i+4}$ correlation between Aib2 and Asp6 was observed along with the Aib2/Cys5 $C^{\beta}H_i \rightarrow NH_{i+3}$ cross peak (Figure S8). At the same time the fingerprint region of

the peptide loop in the NOESY spectrum noticeably changed with appearance of the signals due to the $C^{\alpha}H_i \rightarrow NH_{i+3}$ interactions Cys5/Ile7, Asp6/Val9, Asp6/Nle10, Nle10/Glu12 and disappearance of the long-range cross peak Cys5/Trp11, probably, because of the involvement of Cys5 residue in the helix. Thus, the helix-promoting influence of Aib2 residue extends up to N-terminal part of the loop and, apparently, changes the conformation of its C-terminal portion to maintain the cyclic peptide structure.

NOESY spectrum of **Aib8** showed that C^{α}-tetrasubstituted Aib residue involved in the helical conformation the central part of the peptide loop with maintenance of the vicinity of Cys5 and Trp11 residues like in the parent peptide **v114*** (Figure 3, C). In the aliphatic/NH region of the NOESY spectrum we observed medium-range correlations that comprised residues from Aib8 to Glu12: two $C^{\beta/\gamma}H_i \rightarrow NH_{i+3}$ (Aib8/Trp11 and Val9/Glu12) correlations and a $C^{\beta}H_i \rightarrow NH_{i+4}$ (Aib8/Glu12) cross peak can be identified in the spectrum (Figure S11). Moreover, the helix-promoting effect of Aib was seen also in the N-terminal part of the peptide with the appearance of the signal due to the vicinity of Asn4 and Aib8. Thus, Aib residue induces a helix formation rather than a simple turn in the peptide loop.

In the fingerprint region of the NOESY spectrum of **Aib12** a set of strong medium-range correlations involving residues from Ile7 to Cys15 can be identified, in particular, two $C^{\alpha}H_i \rightarrow NH_{i+3}$ (His8/Trp11 and Nle10/Trp13) and two $C^{\alpha}H_i \rightarrow NH_{i+4}$ (Ile7/Trp11 and Trp11/Cys15) cross peaks can be seen (Figure 3, D). The medium-range interaction between Ile7 and Trp11 was also observed in the aliphatic/NH region (Figure S14). The amide proton region contained most of the sequential $N\text{-}H_i \rightarrow N\text{-}H_{i+1}$ correlations in the region comprising the segment 9-19 of **Aib12** suggesting the adoption of a helical conformation stabilized in this region. Similarly to **Aib2** no signal due to the vicinity of Cys5 and Trp11 was found in this case, because of the involvement of Trp11 in the helical structure and the influence of Aib that extended up to the C-terminal part of the peptide loop. However, an increase of the flexibility was observed for the N-terminal segment.

Thus, NMR data confirmed the conformational constrain induced by the presence of Aib in its adjacent region. In particular, the stabilization of helical structure was observed in the N-terminal and C-terminal segments of **Aib2** and **Aib12**, respectively, with corresponding conformational changes of the peptide loop to maintain the overall cyclic peptide structure. Interestingly, in the case of **Aib8** the insertion of Aib did not lead to an increase of turn rigidity, but promoted helix formation in the central part of the peptide.

To study the resistance of the peptides to the enzymatic degradation, stability in vitreal environment was carried out by incubating the peptides in porcine vitreous at 37°C. The

introduction of the non-proteinogenic C^{α}-tetrasubstituted amino acid into the structure of most peptides significantly increased their stability in comparison to the peptides containing only coded amino acids (Figure 4).

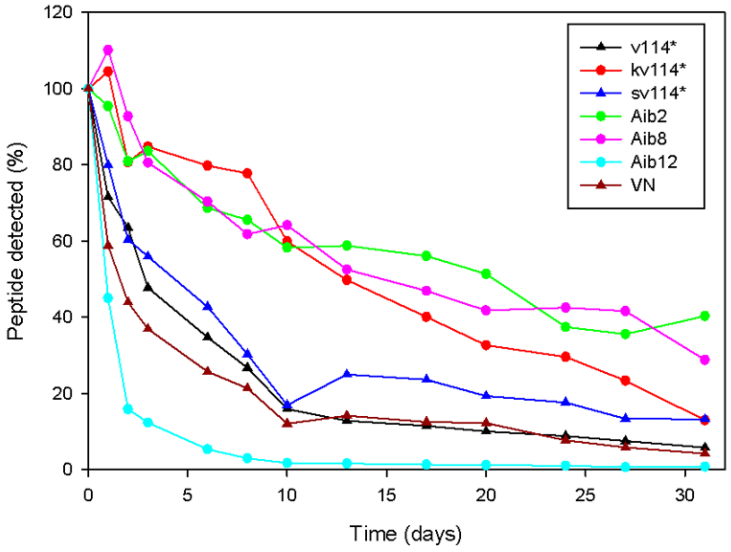

Figure 4. Peptide stability in porcine vitreous. The peptides were incubated with porcine vitreous and the stability was determined by measuring their concentration at different time intervals using UPLC-MS/MS.

The lifetime of Aib-containing peptides in porcine vitreous increased by 7-10 times, compared to the parent peptide **v114***, with the only exception of **Aib12** that disappeared after 10 days and showed to be less stable in solution than **v114***.

Cytotoxicity of the peptides was evaluated by MTT assay. Most of the peptides were not toxic to the ARPE-19 cells at concentrations up to 20 μM (Figure S15). These results confirm the potential of the Aib-containing analogs of **v114*** as promising ocular anti-VEGF compounds.

The affinity of the peptides to VEGF was studied by means of microscale thermophoresis (MST) both immediately after peptide and protein mixing and after 30 min incubation of the peptide/VEGF mixture in order to reach the equilibrium state of the complex. MST data without incubation showed that complete removal of the N-terminal tail significantly reduced the ability of **v114*** to bind vascular endothelial growth factor (Table 2).

Table 2. The affinity of the peptides to vascular endothelial growth factor

Entry	Compound	K_D, nM (no incubation)	K_D, nM (with incubation)
1	**v114***	3870 ± 40	300 ± 75
2	**Aib2**	2970 ± 30	4 ± 1
3	**Aib8**	11800 ± 140	not determined
4	**Aib12**	940 ± 20	150 ± 4
5	**kv114***	540 ± 20	3000 ± 263
6	**sv114***	9970 ± 180	not determined
7	**VN**	1940 ± 40	not determined
8	**Bevacizumab**	not determined	4 ± 1

However, the elimination of only glutamic acid and proline in the peptide **VN** led to a two-fold increase of the affinity. This observation evidences the influence of the N-terminal tail despite the absence of the direct interaction with VEGF, that was shown by β^3-substitutions.[14] The introduction of Aib into the peptide sequence favored VEGF binding with corresponding K_D decrease. This is in accordance with the hypothesis of Reille-Seroussi[15] about the importance of the conformational constrain for tight VEGF binding. However, in the case of histidine/Aib substitution at position 8, where the parent peptide adopts a turn conformation, the affinity to VEGF decreased dramatically (Entry 3, Table 2). Apparently, the formation of the rigid helical structure instead of the turn in the peptide loop prevented its interaction with VEGF.

The affinity the Aib-containing peptides that showed the strongest VEGF-binding was evaluated after incubation of the mixture before carrying out the MST measurement. In most of the cases a strong K_D decrease was observed. This can be due to the time necessary to the peptides to reach the binding site of the VEGF molecule. However, in the case of **kv114*** an opposite behavior was seen. Probably, the time-dependent decrease of the affinity is caused by a conformational rearrangement of the bound peptide and the repulsion of the positively charged N-terminal amino groups. On the contrary, Aib2 with similar structure but without N-terminal lysines showed an affinity similar to those of bevacizumab with K_D in the nanomolar range.

A correlation between VEGF signaling inhibition and dissociation constants of the peptides obtained by MST and cell-based assay was observed (Figure 5, Table 3).

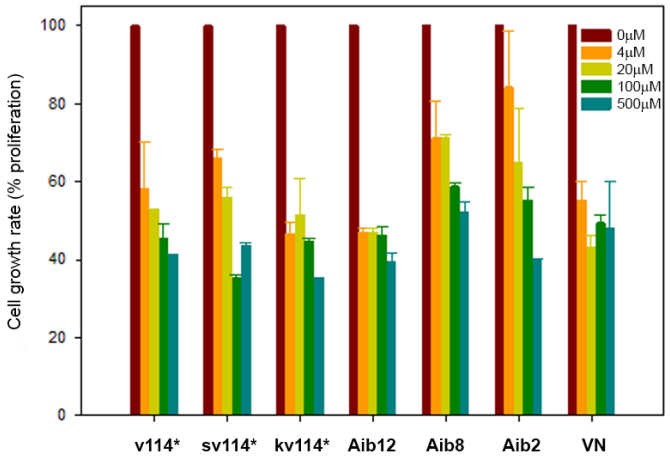

Figure 5. Inhibition of VEGF induced proliferation of HUVEC cells in the presence of anti-VEGF peptides.

Table 3. VEGF-induced proliferation of HUVECs in the presence of the peptides and bevacizumab

Entry	Compound	IC_{50}, μM
1	**v114***	20.0
2	**Aib2**	10.0
3	**Aib8**	50.0
4	**Aib12**	3.5
5	**kv114***	6.0
6	**sv114***	12.0
7	**VN**	4.0
8	**Bevacizumab**	0.001

IC_{50} values for anti-VEGF antibody bevacizumab and **v114*** were 1 nM and 20 μM, respectively, that was in line with the results obtained by Haase et al.[14] The more potent VEGF inhibition by monoclonal antibody, can be explained by its larger VEGF binding surface, than that of the peptide. **Aib8** with constrained loop lost VEGF inhibition ability as compared to the parent peptide **v114***. On the contrary, **VN** with shortened N-tail showed stronger VEGF-binding, that confirmed the importance of N-terminal residues for the stabilization of the peptide conformation necessary for the interaction with VEGF molecule. The insertion of N- or C-terminal Aib-residue provided the increase of the affinity to vascular endothelial growth factor. It is particularly evident

for the peptides **Aib12** and **kv114***. Interestingly, in the later case the peptide showed stronger VEGF inhibition than **Aib2** with similar structure, probably, due the interaction of the peptide/VEGF complex with negatively charged cell surface or other cell culture components and its elimination from the system, as in the case of chemokine inhibitors described in our previous work.[25] However, this phenomenon needs more detailed investigation by using, for example, fluorescently labeled peptides to study their distribution. Thus, among the peptides studied, conformationally constrained peptides **Aib2** and **kv114*** showed both high stability in porcine vitreous and strong VEGF binding, that proves their high potential for further development of efficient vascular endothelial growth factor inhibitors.

In summary, herein we report a series of cyclic peptides that contain C^{α}-tetrasubstituted amino acid Aib at different positions. The insertion of Aib into the structure of the parent peptide **v114*** allowed building the conformational constrain at the corresponding sites of the peptide sequence. We found that the induction of N-terminal helical conformation or stabilization of the C-terminal helix could noticeably increase the affinity of these Aib-containing **v114*** analogs to vascular endothelial growth factor. In addition, the insertion of α-aminoisobutyric acid significantly reduced the sensitivity of the peptides to enzymatic degradation and enhanced their stability in vitreal environment. Thus, the Aib-containing peptides are promising candidates for the design and development of the inhibitors with enhanced VEGF binding.

EXPERIMENTAL PART

Iris Biotech: N,N-dimetylformamide (DMF), dichloromethane (DCM), N,N-diisopropylethylamine (DIPEA), trifluoroacetic acid (TFA), piperidine, Rink amide resin; *Sigma Aldrich:* acetonitrile (MeCN) for mass spectrometry (MS) (>99,9%), TFA for MS (>99,9%), diethyl ether, triisopropylsilane (TIS), Fmoc-Aib-OH, ethanedithiol (EDT); *Carbosynth*: ethyl (hydroxyimino)cyanoacetate (OxymePure), (2-(1H-benzotriazol-1-yl)-1,1,3,3-tetramethyluronium hexafluorophosphate (HBTU), *N*-[(dimethylamino)-1*H*-1,2,3-triazolo-[4,5-*b*]pyridin-1-ylmethylene]-*N*-methylmethanaminium hexafluorophosphate *N*-oxide (HATU); *GL Biochem:* Fmoc-Val-OH, Fmoc-Glu(O*t*Bu)-OH, Fmoc-Pro-OH, Fmoc-Asn(Trt)-OH, Fmoc-Cys(Trt)-OH, Fmoc-Asp(O*t*Bu)-OH, Fmoc-Ile-OH, Fmoc-His(Trt)-OH, Fmoc-Nle-OH, Fmoc-Trp(N^{in}Boc)-OH, Fmoc-Phe-OH, Fmoc-Arg(Pbf)-OH, Fmoc-Leu-OH.

Peptide synthesis. The synthesis was carried out on automatic peptide synthesizer Biotage SyroWave. Fmoc-protected Rink amide resin (250 mg; 0.65 mmol/g) was swelled in 2 mL of DMF

in 30 minutes, the solvent was filtered off and Fmoc protective group was removed with 20% piperidine in DMF (2 cycles for 5 and 20 minutes). Then the resin was washed 4 times with 2 mL of DMF and acylation was performed. At each acylation step (1 hour) the 5-fold excess of protected amino acid and HBTU and 7-fold excess of DIPEA was used. In the case of Aib and the following amino acid acylation was performed 2 times with 5 equivalents of HATU and 7 equivalents of DIPEA. After each acylation, the resin was washed 3 times with 2 mL of DMF. The cycles of acylation and Fmoc deprotection were repeated until the desired peptide sequences were obtained. In the case of the peptide **Aib2** the Fmoc removal from Aib residue was carried out with 20% piperidine solution containing 1M OxymaPure. At the end of the synthesis the peptides were cleaved from the resin with 3 mL of the mixture of TFA/water/TIS/EDT (*v/v/v/v* 94/2.5/1/2.5) and precipitated in 5 mL of diethyl ether. The precipitate was centrifuged and dried. The resulting linear peptide was dissolved in 0.15M ammonium bicarbonate solution to a concentration of 1 mg/mL. The solution was stirred for several days until the disulfide bond formation reaction was complete (HPLC-MS control). Then the pH of the resulting solution was adjusted to 2 with 1M hydrochloric acid and the product was purified by preparative HPLC on ÄKTA Pure purification system with UV detection at 224 nm using a C18 Jupiter column (Phenomenex) 21.2 × 250 mm and eluents A: 10 % acetonitrile in water with 0.1% TFA; eluent B: 90% acetonitrile in water with 0.1% TFA. Elution was carried out using a gradient: 0 min - 5% eluent B, 20 min - 31% eluent B; 65 min - 38% eluent B, 70 min - 95% eluent B. Fractions with a purity> 97% were collected and lyophilized. The resulting peptides were analyzed by HPLC-MS (See Supporting Information).

HPLC-MS chromatography: HPLC-MS analyses were performed on Agilent Technologies 1200 instrument in tandem with Agilent 6530 mass accuracy Q-ToF using C18 Pore-shell column (4,6×100 mm). Analytical method: eluent A, TFA/H_2O 0.1% *v/v*; eluent B: TFA/MeCN 0.1% *v/v*; detection at 224 nm; Gradient elution: 0 min – 10% Eluent B, 3 min – 10% Eluent B, 33 min 95% Eluent B, 38 min – 95% Eluent B.

NMR analysis: all NMR experiments were carried out at 298 K in 9:1 (*v/v*) H_2O/D_2O mixture (peptide concentration 1.2 mM) using a Bruker AVANCE Neo spectrometer operating at 600 MHz and the TOPSPIN software package. Water suppression was obtained through excitation sculpting.[31] The homonuclear spectra were acquired by collecting 512 experiments consisting of 64–80 scans and 2 K data points. The spin systems of coded amino acid residues were identified using standard DQF-COSY and CLEAN-TOCSY spectra.[32-34] In the latter case, the spin-lock pulse sequence was

70 ms long. NOESY experiments were utilized for sequence-specific assignment.[35] At the beginning of the experiments the build-up curve of the volumes of NOE cross-peaks as a function of the mixing time (50–500 ms) was obtained in order to avoid the problem of spin diffusion. The mixing time of the NOESY experiment used for interproton distance determination was 150 ms (*i.e.*, in the linear part of the NOE build-up curve).

Circular dichroism (CD) measurements were carried out at 25°C on Jasco J-1500 CD spectrometer (JASCO, Mary's Court Easton, MD, USA) using a Hellma quartz cuvette with an optical pathlenght of 0.1 cm in methanol (MeOH) and phosphate buffer (PBS) at pH 7.0. The spectra were obtained in the wavelength range from 180 to 260 nm and normalized to molar ellipticity per amino acid residue ($[\theta]\times10^{-3}$, $deg\times cm^2\times dmol^{-1}\times res^{-1}$) using the exact peptide concentration obtained from using UV absorption at 280 nm.

Stability of peptides in vitreous fluid. For stability studies, 10 μM of the peptides were mixed with porcine vitreous containing 1% antibiotics (penicillin/streptomycin; Gibco) in Eppendorff tubes. Each time point had designated separate tube. The tubes were incubated at 37°C and the stability of the peptides in vitreal environment was measured by monitoring the concentration of parent peptide at different time point samples using ultra-performance liquid chromatography tandem mass spectrometry (UPLC-MS/MS).

Cytotoxicity study. Cytotoxicity of the anti-VEGF peptides was evaluated using MTT assay as previously described.[36] Briefly, the cells were seeded in 96-well plates at a density of 20.000 cells per well in 150 μL of cell growth medium. After overnight incubation, the cells were washed with PBS. Peptides at various concentrations (0.01–100 μM) in complete cell growth medium (100 μL) were added to each well for incubation (5 h at 37°C, 7% CO_2). Poly-L-lysine (PLL) treated and untreated cells served as negative and positive controls, respectively. After incubation, the medium was aspirated, the cells were washed with PBS and 150 μL of growth medium was added to the cells. Then, the cells were washed with PBS after incubation of 24 h. A mixture of 90 μL of complete growth medium and 10 μL of 5 mg/ml of MTT solution was added to the wells and the plates were incubated for 4 h at 37°C. After incubation, 100 μL of 10% sodium dodecyl sulfate (Merck) in 0.01 M HCl (Sigma-Aldrich) was added to the wells to solubilize formazan crystals followed by overnight incubation at 37°C. Formazan was quantified by measuring absorbance at

570 nm using a spectral scanning multimode plate reader (Varioskan Flash, Thermo Scientific). Viability of the treated cells was compared to the untreated control cells.

VEGF-binding activity of the peptides. The binding affinity of peptides with VEGF was measured using microscale thermophoresis (MST).[37] The NanoTemper Monolith NT.115 Pico device (NanoTemper Technologies GmbH, München, Germany), fluorescently labeled VEGF-RED protein with an initial concentration of 12 mM and Monolith NT.115 Premium Capillaries were used for the study. Binding of the label (NHS-RED) to the protein molecule (VEGF) was performed according to the standard protocol.[38] Interaction measurements were performed at a constant concentration of VEGF-RED (1 nM), varying the concentration of anti-VEGF peptide in the range from 50 μM to 0.5 nM. The intensity of the infrared (IR) laser was adjusted automatically. The peptide-VEGF interaction was detected by studying the change in the fluorescence of the peptide-protein complex under the influence of an IR laser, which is proportional to the thermophoretic mobility of the labeled protein molecules. To calculate the resulting curve and the standard deviation a software MO Affinity Analysis from NanoTemper was used.

Inhibition of cell proliferation. HUVEC cells (VEGF dependent cell line) were seeded in 96-well plates at a density of 25,000 cells per well in 200 μL of cell growth medium containing recombinant human VEGF165 (0.5 ng/mL). After incubating the cells for 48 h, growth medium was removed, cells washed with PBS. Cells incubated for another 24 h in starvation medium (basal medium without VEGF and FBS). Anti-VEGF peptides in the concentration range of 4, 20, 100, 500 μM was pre-mixed with VEGF165 at a concentration of 50 ng/mL and incubated for 2 h at 37°C. After that, cells were treated with peptide and VEGF mixture solution for 48 h. Cells were washed with PBS and inhibition of proliferation was measured by MTT assay. Data were expressed as percent proliferation (optical density of the sample/optical density of the control without peptide) and were fitted by PRISM to yield IC_{50} values for the peptides. Data are represented as ± standard deviation (n = 3).

ASSOCIATED CONTENT

Supporting information

A scheme illustrating the mechanism of diketopiperasine formation during the synthesis of **Aib2**; HPLC profiles and MS data of the peptides; ^{1}H NMR, TOCSY and NOESY spectra; the data on cytotoxicity and MST data for the peptides and bevacizumab.

AUTHOR INFORMATION

Corresponding Author

E-mail: ivan.guryanov1@gmail.com

Notes

The authors declare no competing financial interest.

ACKNOWLEDGMENTS

This work was financially supported by Megagrant #14.W03.31.0025 of the Government of Russian Federation.

REFERENCES

(1) Markovic-Mueller, S.; Stuttfeld, E.; Asthana, M.; Weinert, T.; Bliven, S.; Goldie, K. N.; Kisko, K.; Capitani, G.; Ballmer-Hofer, K. Structure of the full-length VEGFR-1 extracellular domain in complex with VEGF-A *Struct. Des*. **2017**, *25*, 1-12.

(2) Carmeliet, P. Angiogenesis in health and disease. *Nat. Med*. **2003**, *9*, 653-660.

(3) Agarwal, A.; Rhoades, W. R.; Hanout, M.; Soliman, M. H.; Sarwar, S.; Sadiq, M. A.; Sepah, Y. J.; Do, D. V.; Nguyen, Q. D. Management of neovascular age-related macular degeneration. Current state-of-the-art care for optimizing visual outcomes and therapies in development. *Clin. Ophthalmol.* **2015**, *9*, 1001-1015.

(4) Wong, L. W.; Su, X.; Li, Z.; Cheung, C. M.; Klein, R.; Cheng, C. Y.; Wong, T. Y. Global prevalence of age-related macular degeneration and disease burden projection for 2020 and 2040: a systematic review and meta-analysis. *Lancet Glob. Health* **2014**, *2*, e106-116.

(5) Glade-Bender, J.; Kandel, J. J.; Yamashiro, D. J. VEGF blocking therapy in the treatment of cancer. *Expert Opin. Biol. Ther*. **2003**, *3*, 263-276.

(6) Liang, X.; Xu, F.; Li, X.; Ma, C.; Zhang, Y.; Xu, W. VEGF signal system: The Application of antiangiogenesis. *Cur. Med. Chem.* **2014**, *21*, 894-910.

(7) Supuran C. T. Agents for the prevention and treatment of age-related macular degeneration and macular edema: a literature and patent review. *Expert Opin. Ther. Pat.* **2019**, *29*, 761-767.

(8) Holash, J.; Davis, S.; Papadopoulos, N.; Croll, S. D.; Ho, L.; Russell, M.; Boland, P.; Leidich, R.; Hylton, D.; Burova, E.; Ioffe, E.; Huang, T.; Radziejewski, C.; Bailey, K.; Fandl, J. P.; Daly, T.; Wiegand, S. J., Yancopoulos, G. D.; Rudge, J. S. VEGF-Trap: A VEGF blocker with potent antitumor effects. *Proc. Natl. Acad. Sci USA* **2002**, *99*, 11393-11398.

(9) Ghosh, J. G.; Nguyen, A. A.; Bigelow, C. E.; Poor, S.; Qiu, Y.; Rangaswamy, N.; Ornberg, R.; Jackson, B.; Mak, H.; Ezell, T.; Kenanova, V. Long-acting protein drugs for the treatment of ocular diseases. *Nature Comm.* **2017**, *8*, 14837.

(10) D'Andrea, L. D.; Del Gatto, A.; De Rosa, L.; Romanelli, A.; Pedone, C. Peptides targeting angiogenesis related growth factor receptors. *Cur. Pharm. Design* **2009**, *15,* 2414-2429.

(11) Checco, J. W.; Gellman, S. H. Iterative nonproteinogenic residue incorporation yields α/β-peptides with a helix–loop–helix tertiary structure and high affinity for VEGF. *ChemBioChem* **2017**, *18*, 291-299.

(12) Fairbrother, W. J.; Christinger, H. W.; Cochran, A. G.; Fuh, G.; Keenan, C. J.; Quan, C.; Shriver, S. K.; Tom, J. Y. K.; Wells, J. A.; Cunningham, B. C. Novel peptides selected to bind vascular endothelial growth factor target the receptor-binding site. *Biochemistry* **1998**, *37,* 17754-17764.

(13) Fedorova, A.; Zobel K.; Gill, H. S.; Ogasawara, A., Flores, J. E.; Tinianow, J. N.; Vanderbilt, A. N.; Wu, P.; Meng, Y. G.; Williams, S. P.; Wiesmann, C.; Murray, J.; Marik, J.; Deshayes, K. The development of peptide-based tools for the analysis of angiogenesis. *Chem. Biol.* **2011**, *18*, 839-845.

(14) Haase, H. S.; Peterson-Kaufman, K. J.; Lan Levengood, S. K.; Checco, J. W.; Murphy, W. L.; Gellman, S. H. Extending foldamer design beyond α-helix mimicry αβ-peptide inhibitors of vascular endothelial growth factor signaling. *J. Am. Chem. Soc.* **2012**, *134*, 7652-7655.

(15) Reille-Seroussi, M.; Gaucher, J.-F. ; Desole, C. ; Gagey-Eilstein, N. ; Brachet, F. ; Broutin, I. ; Vidal, M. ; Broussy, S. Vascular endothelial growth factor peptide ligands explored by competition assay and isothermal titration calorimetry. *Biochemistry* **2015**, *54*, 5147-5156.

(16) Toniolo, C.; Crisma, M.; Formaggio, F.; Peggion, C. Control of peptide conformation by the Thorpe–Ingold effect (C^{α}-tetrasubstitution). *Biopolymers (Pept. Sci.)* **2001**, *60*, 396-419.

(17) Yasutomi, S.; Morita, T.; Imanishi, Y.; Kimura, S. A molecular photodiode system that can switch photocurrent direction. *Science* **2004**, *304*, 1944-1947.

(18) Guryanov, I.; Moretto, A.; Campestrini, S.; Broxterman, Q.B.; Kaptein, B.; Peggion, C.; Formaggio, F.; Toniolo, C. Turn and helical peptide spacers: Combined distance and angular dependencies in the exciton-coupled circular dichroism of intramolecularly interacting bis-porphyrins. *Biopolymers* **2006**, *82*, 482-490.

(19) Boal, A.K.; Guryanov, I.; Moretto, A.; Crisma, M.; Lanni, E.L.; Toniolo, C.; Grubbs, R.H.; O'Leary, D.J. Facile and E-selective intramolecular ring-closing metathesis reactions in 3(10)-helical peptides: A 3D structural study. *J. Am. Chem. Soc.* **2007**, *22*, 6986-6987.

(20) Gatto, E.; Porchetta, A.; Stella, L.; Guryanov, I.; Formaggio, F.; Toniolo, C.; Kaptein, B.; Broxterman, Q.B.; Venanzi, M. Conformational effects on the electron-transfer efficiency in peptide foldamers based on alpha,alpha-disubstituted glycyl residues. *Chem. Biodivers.* **2008**, *5*, 1263 -1278.

(21) Becucci, L.; Guryanov, I.; Maran, F.; Guidelli, R. Effect of a strong interfacial electric field on the orientation of the dipole moment of thiolated Aib-oligopeptides tethered to mercury on either the N- or C-Terminus. *J. Am. Chem. Soc.* **2010**, *132*, 6194-6204.

(22) Jesper Lau, J.; Bloch, P.; Schaffer, L.; Pettersson, I.; Spetzler, J.; Kofoed, J.; Madsen, K.; Knudsen, L. B. Discovery of the once-weekly glucagon-like peptide-1 (GLP-1) analogue semaglutide. *J. Med. Chem.* **2015**, *58*, 7370-7380.

(23) Varela, A.; Chouinard, L.; Lesage, E.; Smith, S. Y.; Hattersley, G. One year of abaloparatide, a selective activator of the PTH1 receptor, increased bone formation and bone mass in osteopenic ovariectomized rats without increasing bone resorption. *J. Bone Mineral Res.* **2017**, *32*, 24-33.

(24) Pan, B.; Li, B.; Russell, S. J.; Tom, Y. J. K.; Cochran, A, G.; Fairbrother, W. J. Solution structure of a phage-derived peptide antagonist in complex with vascular endothelial growth factor. *J. Mol. Biol.* **2002**, *316*, 769-787.

(25) Guryanov, I,; Cipriani, S.; Fiorucci, S.; Zashikhina, N.; Marchiano, S.; Scarpelli, P.; Korzhikov-Vlakh, V.; Popova, E.; Korzhikova-Vlakh, E.; Biondi, B.; Formaggio, F.; Tennikova, T. Nanotraps with biomimetic surface as decoys for chemokines. *Nanomedicine: NBM* **2017**, *13*, 2575-2585.

(26) Byun, J. B.; Song, I. K.; Chung, Y. J.; Ryu, K. H.; Kang, Y. K. Conformational preferences of X-Pro sequences: Ala-Pro and Aib-Pro motifs. *J. Phys. Chem. B* **2010**, *114,* 14077–14086;

(27) Karle, I. L.; Flippen-Anderson, J. L.; Uma, K.; Balaram, H..; Balaram, P. Peptide design: influence of a guest Aib-Pro segment on the stereochemistry of an oligo-Val sequence-solution

conformations and crystal structure of Boc-$(Val)_2$-Aib-Pro-$(Val)_3$-OMe. *Biopolymers* **1990**, *29*, 1433-1442.

(28) Gerig, J. T.; McLeod, R. S. 2-Methylalanyl-L-prolyl-L-tryptophan. An unexpected result. *J. Org. Chem.* **1976**, *41*, 1653-1655.

(29) Subirós-Funosas, R.; El-Faham, A.; Albericio, F. Use of Oxyma as pH modulatory agent to be used in the prevention of base-driven side reactions and its effect on 2-chlorotrityl chloride resin. *Biopolymers (Pept. Sci.)* **2012**, *98*, 89-97.

(30) Greenfield, N. J. Using circular dichroism spectra to estimate protein secondary structure. *Nat. Protoc.* **2006**, *1*, 2876-2890.

(31) Hwang, T. L.; Shaka, A. J. Water suppression that works. Excitation sculpting using arbitrary wave-forms and pulsed-field gradients. *J. Magn. Res. A* **1995**, *112*, 275-279.

(32) Rance, M.; Sørensen, O. W.; Bodenhausen, G.; Wagner, G.; Ernst R. R.; Wüthrich, K. Improved spectral resolution in COSY ^{1}H NMR spectra of proteins via double quantum filtering. *Biochem. Biophys. Res. Commun.* **1983**, *117*, 479-485.

(33) Bax, A.; Davis, D. G. MLEV-17-based two-dimensional homonuclear magnetization transfer spectroscopy. *J. Magn. Reson.* **1985**, *65*, 355-360.

(34) Griesinger, C.; Otting, G.; Wüthrich, K.; Ernst, R. R. Clean TOCSY for proton spin system identification in macromolecules. *J. Am. Chem. Soc.* **1988**, *110*, 7870-7872.

(35) Wüthrich, K. NMR of proteins and nucleic acids. Wiley, New York, 1986.

(36) Mosmann T. Rapid colorimetric assay for cellular growth and survival: application to proliferation and cytotoxicity assays. *J. Immunol. Methods* **1983**, *65*, 55–63.

(37) Wienken, C. J.; Baaske, P.; Rothbauer, U.; Braun, D.; Duhr, S. Protein-binding assays in biological liquids using microscale thermophoresis. *Nat. Commun.* **2010**, *1*, 100.

(38) Jerabek-Willemsen, M.; Wienken, C. J.; Braun, D.; Baaske, P.; Duhr, S. Molecular interaction studies using microscale thermophoresis. *Assay Drug. Dev. Technol.* **2011**, *9*, 342-353.

FOR TOC ONLY